Novel spectral features in MeV gamma rays from dark matter

Bringmann, T.; Galea, A.; Hryczuk, A.; Weniger, C.

DOI
10.1103/PhysRevD.95.043002

Publication date
2017

Document Version
Final published version

Published in
Physical Review D. Particles, Fields, Gravitation, and Cosmology

PHYSICAL REVIEW D **95,** 043002 (2017)

Novel spectral features in MeV gamma rays from dark matter

Torsten Bringmann,[1,*] Ahmad Galea,[1,†] Andrzej Hryczuk,[1,‡] and Christoph Weniger[2,§]

[1]*Department of Physics, University of Oslo, Box 1048 NO-0316 Oslo, Norway*
[2]*GRAPPA, Institute of Physics, University of Amsterdam, Science Park 904, 1090 GL Amsterdam, Netherlands*

(Received 25 October 2016; revised manuscript received 8 December 2016; published 16 February 2017)

Astrophysical searches for gamma rays are one of the main strategies to probe the annihilation or decay of dark matter particles. We present a new class of distinct sub-GeV spectral features that generically appear in kinematical situations where the available center-of-mass energy in such processes is just above threshold to produce excited meson states. Using a Fisher forecast with realistic astrophysical backgrounds, we demonstrate that for upcoming experiments like e-ASTROGAM and ComPair these signals can turn out to be the smoking gun in the search for particle dark matter.

DOI: 10.1103/PhysRevD.95.043002

I. INTRODUCTION

Gamma rays provide a promising way of identifying the nature of dark matter (DM), not the least because they may carry distinct spectral features that would provide a smoking-gun signal against dominant astrophysical backgrounds [1]. Those features are expected at the highest kinematically accessible energies from DM annihilation or decay, and hence at GeV to TeV energies for DM candidates that arise in theories extending the electroweak sector of the standard model of particle physics. In this energy range, the most stringent limits on monochromatic, or "line", features are presently provided by observations of the Galactic center (GC) region and halo [2,3]. At much lower energies, in the keV range, monochromatic photons may arise from the decay of sterile neutrinos, another excellent DM candidate [4,5]. There are, however, also nuclear transitions that produce X-ray lines in this energy range, which must be carefully modeled in order not to be confused with a signal (for a recent and still controversial hint of such a signal, see Refs. [6,7]).

While these two energy bands have received a lot of attention in the context of DM searches, energies in the MeV range have so far been studied in much less detail—though early work argued that observable quasi-monochromatic photons at these energies may result from DM annihilation to quarkonium [8,9], as well as step-like features from the decay $b \to s + \gamma$ or $b' \to b + \gamma$, where b' is a hypothetical 4th generation quark [10]. Another possibility is the decay of DM candidates like the gravitino, which has motivated a dedicated line search with the Fermi Large Area Telescope down to energies of 100 MeV [11]. It was also pointed out that for DM lighter than around 100 MeV, the only kinematically accessible nonleptonic states are photons and neutral pions, leading to clear gamma-ray signatures to look for [12–14]. At those energies, however, there is a significant "MeV gap" [15] in the sensitivity of operating and past experiments, such that presently only very weak limits on DM signals exist in this range [16].

There is already a strong interest in the astrophysics community to finally fill this MeV gap, via planned missions like e-ASTROGAM [17] and ComPair [18], in order to address a broad key science program ranging from the physics of ultra-relativistic jets to a better understanding of the Galactic chemical evolution. Here, we point out a new class of potential smoking-gun signatures for DM signals in the range 10 MeV $\lesssim E_\gamma \lesssim$ 100 MeV, providing further motivation for the realization of such missions. These signatures involve transitions between meson states and, in their simplest realization, do not require any new physics (beyond, obviously, the DM particle itself) but inevitably arise in certain kinematical situations for GeV-scale DM annihilating or decaying to heavy quarks. Unlike direct detection or collider experiments, these signatures are thus very sensitive to DM coupling with third or second generation quarks.

This paper is organized as follows. We first briefly review the standard arguments for a featureless gamma-ray spectrum from DM, and then illustrate for the case of B and D mesons how the production and decay of excited meson states can change the picture at sub-GeV photon energies. We then adopt the characteristics of planned experiments in the MeV range for a detailed Fisher forecast, demonstrating that the spectral features identified here can significantly help to discriminate DM signals from astrophysical backgrounds. We move on to discuss further expected features in this energy range and then present our conclusions, along with an outlook for future directions of investigation. In two appendices we assess the impact of the assumed experimental settings and provide details about the adopted Fisher forecast.

*torsten.bringmann@fys.uio.no
†ahmad.galea@fys.uio.no
‡a.j.hryczuk@fys.uio.no
§c.weniger@uva.nl

II. MESON SPECTROSCOPY WITH DARK MATTER

The annihilation or decay of DM typically produces, through decay and fragmentation of the final state particles, a large number of neutral pions with energies all the way up to what is kinematically accessible in a given process. Those pions decay dominantly via $\pi^0 \to \gamma\gamma$, resulting in two monochromatic photons with $E_\gamma = m_{\pi^0}/2$ in the respective pion's rest frame. When boosted to the DM frame, taking into account the high multiplicity of the pions, this leads to a featureless gamma-ray spectrum that is almost indistinguishable among all quark and weak gauge boson final states [1].

In this paper we point out that there are interesting exceptions to this simple, yet widely spread picture. In fact, this should not come as a surprise in view of the highly complicated multistep decay and fragmentation cascades that actually take place in a given annihilation or decay process and which must be simulated with event generators like PYTHIA [19,20] or HERWIG [21] to arrive at general conclusions like the one just quoted. Concretely, heavier mesons and baryons are formed as soon as allowed by kinematics, with the former, requiring only two quarks to combine, being much more abundant than the latter. In the ground state, heavy mesons mostly decay directly to lighter mesons and leptons [22], leading to cascades that eventually result in pions. Large mass hierarchies, furthermore, generally imply that intermediate states in such showering process are produced with high virtuality, which in turn leads to a large probability of gluon emission and therefore again high multiplicities of lighter states [23–25].

If, on the other hand, a meson containing heavy quarks is produced in an excited state, it will typically de-excite before decaying to a lighter meson type with a different quark content—most often by emitting a monochromatic photon or pion. In both situations a clear spectral features arises in the DM rest frame: due to the nonzero kinetic energy of the excited meson, the monochromatic photon leads to a box-shaped spectrum roughly centered on the energy difference between the meson states:

$$\frac{dN}{dE_\gamma} = \frac{1}{E_{\max} - E_{\min}} \theta(E_\gamma - E_{\min})\theta(E_{\max} - E_\gamma), \quad (1)$$

where θ is the Heaviside function and $E_{\max,\min} = E'_\gamma(E^*/M^*)(1 \pm \beta)$. Here, E^* and M^* are the energy and mass of the excited meson (in the DM frame) and $\beta = (1 - M^{*2}/E^{*2})^{1/2}$ its velocity; $E'_\gamma = \Delta M(1 - \Delta M/(2M^*))$ is the photon energy in the decaying meson frame and ΔM the mass difference to the ground state. Photons from $\pi^0 \to \gamma\gamma$, on the other hand, give a bump centered on half of this energy. Both features become wider with larger kinetic energy of the initial meson; in practice, they are sufficiently pronounced only in situations where the excited meson is nearly at rest. In this situation, the location and shape of the resulting spectral features in gamma rays does not only allow for an accurate determination of the DM mass, but in principle also provides a direct way of inferring both the initial meson state and the de-excitation channel.

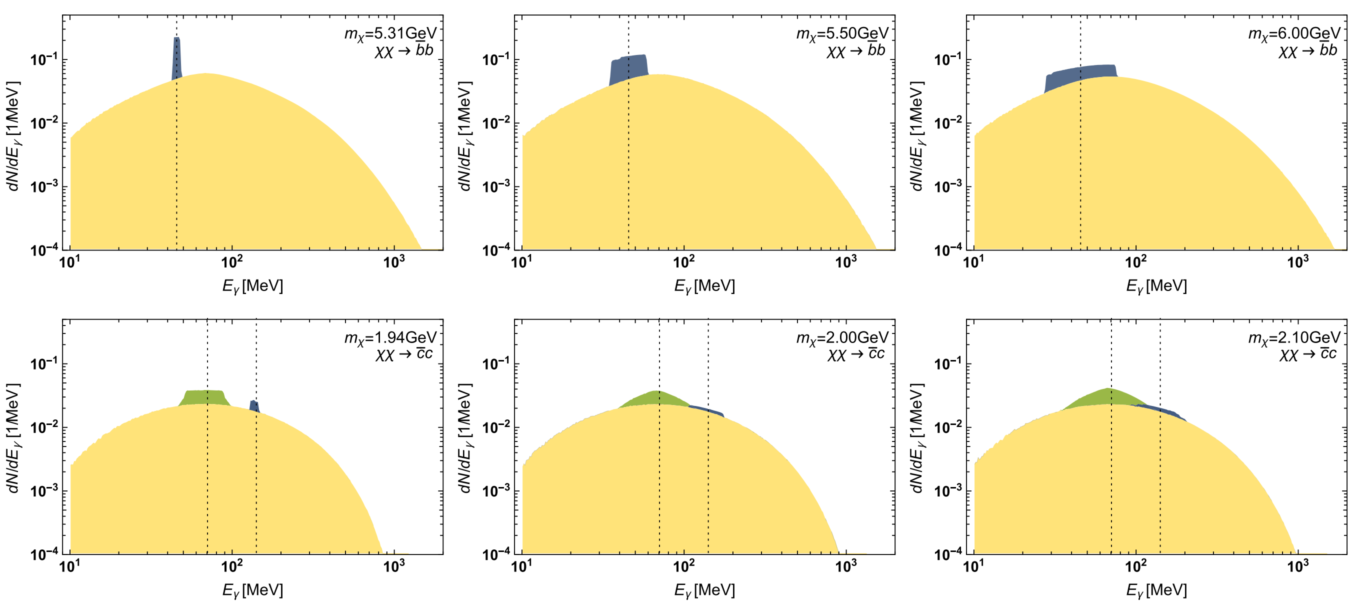

FIG. 1. (Top row) Gamma-ray spectra from $\chi\chi \to \bar{b}b$, for increasing DM mass m_χ (from left to right). The light shaded part is the standard continuum contribution, dominated by π^0 decay. The dark shaded feature results from the decay of excited B meson states, $B^* \to B + \gamma$; the vertical dashed line indicates the corresponding average mass difference $\Delta M_B \equiv 0.046$ GeV. (Bottom row) Same, but for $\bar{c}c$ final states. The two pronounced features here arise from excited D mesons, namely $D^* \to D + \pi^0$, $\pi^0 \to \gamma\gamma$ (left) and $D^* \to D + \gamma$ (right). The latter is roughly centered on $\Delta M_D \equiv 0.142$ GeV, the former on $\Delta M_D/2$.

III. EXAMPLE SPECTRA

In order to illustrate these considerations, let us now concentrate on DM annihilation to $\bar{b}b$ or $\bar{c}c$. In this case virtually every resulting shower will contain at least one B or D meson, respectively, from the hadronization of one of the final state particles with a light quark. The relevant excited B meson states are mostly B^{-*} and B_0^*, which decay by emitting a photon with energy $m_\gamma = m_{B^{-*}} - m_{B^-} = 0.046$ GeV and $m_\gamma = m_{B_0^*} - m_{B_0} = 0.045$ GeV [22]. The mesons (D^{-*}, D_0^*, D_s^{-*}), on the other hand, decay via both decay channels discussed above to the respective ground state; this produces neutral pions and photons with an energy of (0.140,0.142,0.144) GeV and branching ratios of $\mathrm{BR}_{D^*\to D\pi^0} \approx 2/3$ and $\mathrm{BR}_{D^*\to D\gamma} \approx 1/3$ [22].

In Fig. 1, we show the resulting photon spectra for DM annihilation into $\bar{b}b$ and $\bar{c}c$, for a number of benchmark values for the DM mass (the same spectra arise for the decay of a DM particle with twice the stated mass). In order to produce these plots, we ran PYTHIA v8.215 [26] to simulate 10^6 events with an initial state back-to-back $\bar{q}q$ pair and a center-of-mass energy of $2m_{\mathrm{DM}}$, adopting default tuning settings and including both photon and gluon final state radiation. The expected box features around $E_\gamma \simeq \Delta m$ from monochromatic photons are clearly visible, as well as—for the case of $\bar{c}c$ final states—a second feature around $E_\gamma \simeq \Delta m/2$ from monochromatic neutral pions. These features appear on top of the dominant contribution from photons that results from π^0 produced at all energies in the fragmentation process. Increasing the DM mass, the new spectral features that we have reported here broaden and relatively quickly become indistinguishable from the standard pion bump.

IV. DETECTING FEATURES IN THE MEV GAP

There is a pronounced interest of the gamma-ray astronomy community to improve the coverage of sub-GeV photon energies. During the last years, this has culminated in two active efforts for medium-sized satellite missions. Firstly, e-ASTROGAM [17], which is proposed as an ESA M5 mission by the European community, and secondly, ComPair [18], which is a proposal mostly carried by the US community. In order to assess the expected detection significance of the spectral features described above, in the following,we adopt the preliminary characteristics of these detectors as summarized in Table I and perform a Fisher forecast. The Fisher forecast takes into account the full covariance matrix of the spectral analysis, for which convenient analytical expressions are presented in Ref. [27].

We model the differential flux by $\phi(E,\vec{\theta}) = \phi_{\mathrm{sig}} + \phi_{\mathrm{bg}}$, where $\vec{\theta}$ are the model parameters. The model is assumed to be linear in $\vec{\theta}$. The Fisher information matrix for a spectral analysis and parameters θ_i and θ_j is then given by (see Appendix B and Ref. [27])

TABLE I. Adopted characteristics for upcoming or planned instrument in the pair-production regime for the 10–3000 MeV energy range (10–1000 MeV in the case of ComPair). For the energy resolution, we adopt the value at 100 MeV close to the spectral features of interest. For the adopted ROI, the finite angular resolution is irrelevant. We assume survey mode with equal sky coverage throughout.

Experiment	$\Delta E/E$	FoV [sr]	A_{eff} [cm^2]	T_{obs}
e-ASTROGAM [17,28]	25%	2.5	1500	5 yr
ComPair [18]	12%	3	1000	5 yr

$$\mathcal{I}_{ij} = T_{\mathrm{obs}} A_{\mathrm{eff}} \int_{E_{\min}}^{E_{\max}} dE \frac{\partial_i \phi(E) \partial_j \phi(E)}{\phi_{\mathrm{bg}}(E)} + \delta_{ij} \frac{1}{\Sigma_i^2}, \quad (2)$$

where T_{obs} is the observation time, $\partial_i \phi(E)$ denotes the change in the differential flux as function of parameter θ_i, and $\phi_{\mathrm{bg}}(E)$ is the expected observed flux (assumed to be dominated by the background). As the energy range, we always adopt $E_{\min}, E_{\max} = 10$ MeV, 1 GeV, to allow for an easy comparison between instruments. Lastly, Σ_i^2 refers to the external variance of parameter θ_i, e.g. from additional external knowledge of the background systematics.

We model the background with the three components shown in Fig. 2, taken from Ref. [29]. Our region of interest (ROI) is a $20° \times 20°$ region around the GC; we approximate its intensity by the more extended ROI used in [29]. In the Fisher analysis, we allow not only the normalization of each of the three components to vary, but also their slopes and the curvatures. Hence, our complete background model reads $\phi_{\mathrm{bg}} = \sum_{i=1}^{3} (\theta_i^n + \theta_i^s \log(E/E_0) + \theta_i^c \log(E/E_0)^2)\phi_i$, where $i = 1$, 2, 3 refers respectively to inverse Compton scattering (ICS), bremsstrahlung and the astrophysical π^0 contribution; $E_0 = 0.3$ GeV is a pivot point, and ($\theta_i^n = 1$, $\theta_i^s = \theta_i^c = 0$) describe the baseline model. For the external variance of the background parameters, we assume standard

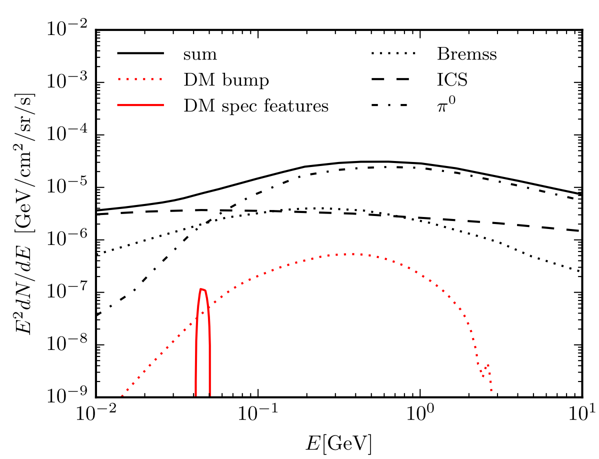

FIG. 2. Backgrounds [29] and one variant of the signal spectra used in the current analysis ($\chi\chi \to \bar{b}b$ with $m_\chi = 5.3$ GeV).

deviations $\Sigma_{\theta_i^n} = 0.5$, $\Sigma_{\theta_i^s} = 0.15$ and $\Sigma_{\theta_i^c} = 0.05$. These numbers imply that, within 2σ variance, the background model can vary by roughly a factor two in the considered energy range. This is adopted *ad hoc*, and more accurate estimates can only be made once data is available. Our qualitative conclusions are relatively insensitive to this number.

The signal is modeled by two components as also shown in Fig. 2, $\phi_{\rm sig} = \sum_{i=4}^{5} \theta_j \phi_i$, where $i = 4$, 5 corresponds respectively to the broad pion bump and the spectral features visible in Fig. 1. In the case of $\bar{c}c$ final states, we treat the two spectral features together. For the sake of this figure, the spectra are normalized to a reference cross section of $\langle\sigma v\rangle = 10^{-26}\ \mathrm{cm^3\,s^{-1}}$. We adopt a standard Navarro-Frenk-White (NFW) profile with a scale radius 20 kpc, 0.4 $\mathrm{GeV\,cm^{-3}}$ local density and 8.5 kpc distance to the GC (see Ref. [1] for details). The corresponding J-value integrated over the ROI is $5.0 \times 10^{22}\ \mathrm{GeV^2\,cm^{-5}}$.

In total we are thus dealing with an 11 parameter model. The expected variance of the DM signal normalization parameters is $\sigma_{ii}^2 = (\mathcal{I}^{-1})_{ii}$, with $i = 4$, 5. Here, $\mathcal{I}^{-1}$ denotes the inverse of the 11×11 Fisher information matrix. Note that the matrix inversion fully takes into account correlations between background and signal components in the model. The projected 95% CL upper limit on the annihilation cross section into spectral features is then $\langle\sigma v\rangle_{\rm UL} = 1.65 \cdot \sigma_{55} \cdot 10^{-26}\ \mathrm{cm^3\,s^{-1}}$ (see Appendix B).

V. RESULTS

Our results for the projected upper limits are summarized in Fig. 3. Here, we consider for illustration only ComPair; see the supplemental material for similar results for

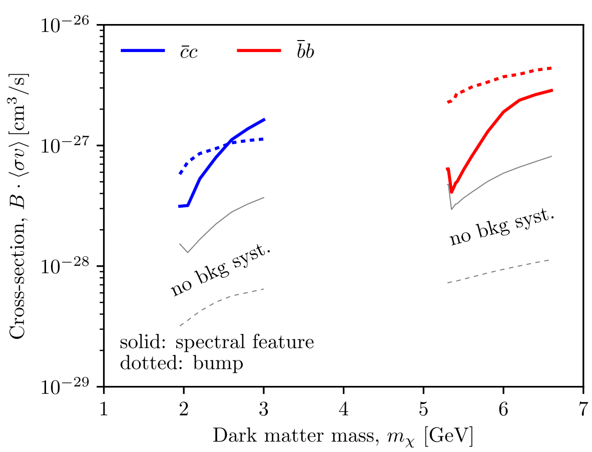

FIG. 3. The solid and dotted red and blue lines show projected 95% CL upper limits on the spectral features as well as the pion bump, including our estimate for the background systematics, for the ComPair satellite. We also show (in gray) results obtained when neglecting background systematics. For profiles steeper than NFW, and an optimized ROI, $B \sim 10$ is possible (see text for discussion).

e-ASTROGAM. We show the projected 2σ upper limits that could be obtained for DM masses close to the kinematic cutoff for the indicated quark channels.

We find that, indeed, after taking into account a realistic model for background uncertainties, the spectral features (solid lines) have a larger constraining power than the broad pion bump (dotted lines). If one were to completely neglect background systematics (light gray lines), one would falsely conclude that the pion bump is more constraining. Note that at very small masses the limits on the spectral features become slightly less constraining again; this is because some of the excited meson states are no longer kinematically accessible.

VI. DISCUSSION

While our projected limits from the pion bump alone would already be competitive with present bounds from dwarf galaxy observations by the Fermi gamma-ray space telescope [30], including the spectral features in the analysis would significantly improve them. Let us stress, however, that Fig. 3 mainly serves to illustrate the relative importance of the two signal contributions in setting the limit. Rather than the annihilation rate $\langle\sigma v\rangle$, we hence plot $B\langle\sigma v\rangle$, where $B = 1$ corresponds to the specific analysis settings described above. Both a data-optimized ROI (see, e.g. [31]) and a DM profile steeper than NFW would easily increase B by a factor of a few, allowing ComPair or e-ASTROGAM to detect the spectral features described here even if there is no hint for a signal in dwarf galaxy observations.

Concerning possible spectral features, the B and D meson families we have focused on here have the advantage of de-exciting via the emission of a single photon or neutral pion. Furthermore, while DM annihilation or decay can directly produce such excited states with small kinetic energies, this is not expected for astrophysical processes. Let us stress, however, that the spectra shown in Fig. 1 are just examples for similar features that may arise at sub-GeV energies.

The dark sector may, e.g., feature a non-Abelian gauge symmetry with confinement [32]. The dominant final states of DM annihilation would then naturally be dark meson states that de-excite by emitting a dark pion $\tilde{\pi}$. If $\tilde{\pi}$ dominantly decays to two photons, this would lead to identical features as for the decay of a standard π^0—with the difference that these features could in principle appear at any energy because the differences in energy levels follow from the physics of the dark and not the visible sector. As noted earlier [8–10], DM annihilation to bound quark-antiquark states also leads to potential smoking-gun signatures if accompanied by the emission of a (necessarily quasi-monochromatic) photon. We therefore expect further identifiable features if the quarkonium is not produced in its ground state or if the coproduced boson is a π^0 rather than a photon. While this adds yet another promising type of sub-GeV spectral features to our list, a full classification of the potentially rich phenomenology is beyond the scope of the present work.

Let us finally stress that codes like PYTHIA are tuned to higher energies, where the formation of the $\bar{q}q$ pair and the subsequent hadronization can be treated as separate processes. This clearly introduces a certain theoretical error, warranting more detailed studies about meson production at threshold (as well as direct quarkonium production, see the discussion above, which is not covered by PYTHIA). On the other hand, we note that spectral features like the ones shown in Fig. 1 arise mainly due to kinematics, because only a few meson states are kinematically accessible and the de-excitation time scale is shorter than the decay time scale. For that reason, we do not expect that an improved estimate of the dynamics of meson production will lead to qualitative differences in the relative normalization of the spectral components.

VII. CONCLUSIONS AND OUTLOOK

The clear identification of a DM signal above astrophysical backgrounds generally proves to be a big challenge, and finding distinct spectral features on top of an observed smooth excess could be central to such an endeavour. In this paper, we have pointed out a potentially large class of such spectral features in the almost unexplored sub-GeV energy range. By means of a Fisher forecast, which in the way it is implemented here introduces a new method in the context of indirect DM searches [27], we verified that missions like ComPair and e-ASTROGAM could indeed sufficiently reduce the astrophysical background uncertainties to identify such a smoking-gun signature for GeV particle DM.

We note that the possibility to probe light DM is also interesting because of the strongly limited sensitivity of direct detection experiments in this mass range [33] (though there are various ideas to overcome these difficulties, e.g. [34–38]). The features reported here have, furthermore, the potential to directly probe—and in fact disentangle—DM couplings to 2nd or 3rd generation quarks, for which both collider and direct DM searches are generally less sensitive. Let us finally stress that mesons do not only decay via photons and neutral pions; this may lead to corresponding spectral features also in other indirect detection channels, notably positrons and neutrinos. Taken together, this points to a potentially rich DM phenomenology at sub-GeV energies which will open promising avenues for future studies.

ACKNOWLEDGMENTS

We thank Richard Bartels, Lars Bergström, Lars Dal, Aldo Morselli, Julie McEnery and Are Raklev for very fruitful discussions. A. H. is supported by the University of Oslo through the Strategic Dark Matter Initiative (SDI). C. W. is supported by the Netherlands Organization for Scientific Research (NWO) through a Vidi grant.

APPENDIX A: EXPERIMENTAL SENSITIVITY TO MEV FEATURES

In the main text, we have explicitly shown the projected experimental sensitivity only for the ComPair satellite, with adopted experimental characteristics as summarized in Table I. Here, we complement this by discussing the analogue to Fig. 3 also for the e-ASTROGAM mission and a fiducial future experiment with even better performance.

1. e-ASTROGAM

In Fig. 4, we show the projected upper limits for e-ASTROGAM, assuming experimental characteristics as summarized in Table I. For a naive analysis, which does not include the effect of background systematics, these limits are essentially identical to those of ComPair (to within 10%, except for the close-to-threshold limits for the $\bar{b}b$ channel where the difference is slightly larger). This is expected because the grasps of the two instruments are very similar.

Once we include the background systematics, however, ComPair is clearly somewhat better suited to distinguish DM signal features at MeV energies than e-ASTROGAM. This is because it has an energy resolution that is almost twice as good, which helps to identify both the broad and the narrow spectral feature in the DM signal. However, given that the relevant spectral features are not more narrow than about 10% for most of the parameter space shown in the figure, which is comparable to the energy resolution of ComPair, the difference in general remains small—except

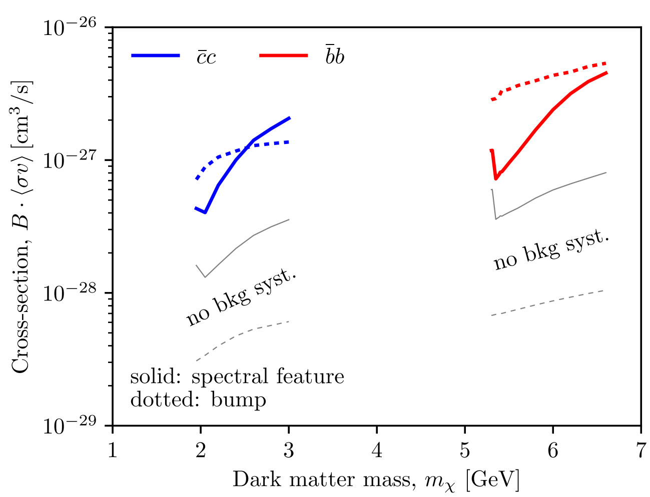

FIG. 4. Same as Fig. 3 but for experimental characteristics corresponding to e-ASTROGAM.

for the line-like feature in the $\bar{b}b$ final state for $m_\chi \lesssim 5.5$ GeV, where ComPair becomes more sensitive by up to a factor of 2.

We finally note that for both, ComPair and e-ASTROGAM, we use the energy range 10 MeV–1 GeV in our analyses. This allows an easy comparison of the results. However, we find that the projects constraints on the continuum component of the DM signal significantly depend on the high-energy cutoff. If we extend the energy range up to 3 GeV, the e-ASTROGAM limits strengthen by a factor of up to three for $\bar{c}c$ final states, and by less than two for $\bar{b}b$ final states. The projected limits for the line component change only very mildly.

2. IDEALIZED GAMMA-RAY EXPERIMENT

Let us now assess by how much the situation could be improved for an idealized future experiment, for which we assume an effective area of $A_{\rm eff} = 10^4$ cm^2 (again for an exposure of 5 years) and an energy resolution of 1%. The resulting projected upper limits are shown in Fig. 5.

As expected, the limits excluding the effect of background systematics simply improve by a factor of roughly 3, compared to our projections for ComPair, corresponding to the square root of the increase in exposure. It also becomes clear that increasing the energy resolution beyond 10% has no impact on the continuum limits, even when taking into account background systematics. For the spectral features we are interested in here, however, a better energy resolution would indeed imply even better detectional prospects. Taken at face value, this would allow us to constrain the $\bar{b}b$ channel for DM annihilation just above threshold by almost two orders of magnitudes more stringently than current limits [30].

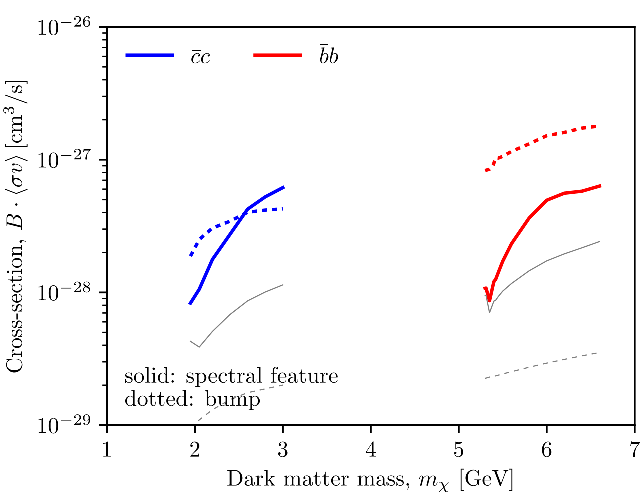

FIG. 5. Same as Fig. 3 but for an idealized future experiment with 1% energy resolution and an effective area 10 times that of ComPair.

APPENDIX B: FISHER FORECAST

Fisher forecasting is a common method for experimental design, and extensively used in, e.g. the cosmology community [39–41]. It is based on the Fisher information matrix, which is a measure of the information that an observation is expected to carry about a set of unknown parameters. However, its use in the indirect and direct DM detection communities is up to now rather limited (see, e.g. Ref. [42] for previous examples). Here, and to the best of our knowledge for the first time, we adopt some new and simple expression for the calculation of the Fisher information matrix that can be used for predicting sensitivities of any counting experiment in the large-number limit.

Let us first briefly summarize the derivation of Eq. (2), before we illustrate how to translate projected limits to detection sensitivities in the particular case we are interested in here. The full details and a few examples are presented elsewhere [27]. The starting point is the unbinned Poisson likelihood function

$$\mathcal{L}(\boldsymbol{\theta}|\mathcal{D}) = e^{-\mu_{\rm tot}(\boldsymbol{\theta})} \prod_{i=1}^{n_{\rm ev}} \Phi_{\rm tot}(E_i|\boldsymbol{\theta}), \tag{B1}$$

where θ denotes the model parameters, $\mu_{\rm tot}$ the total predicted number of events, $i = 1, \ldots, n_{\rm ev}$ runs over the number of measured photons, $\Phi_{\rm tot}(E_i|\theta)$ is the differential number of expected photons, and E_i is the energy of photon i. Furthermore, $\Phi_{\rm tot}$ is related to the physical flux by $\Phi_{\rm tot} = T_{\rm obs} A_{\rm eff} \phi_{\rm tot}$, where $T_{\rm obs}$ and $A_{\rm eff}$ denote observation time and instrument effective area, respectively. Furthermore, we assume that the model is linear,

$$\Phi_{\rm tot}(E|\boldsymbol{\theta}) = \sum_{k=1}^{n_{\rm comp}} \theta_k \Phi_k(E). \tag{B2}$$

The Fisher information matrix is defined as the expected value of the second moment of the score, i.e. the gradient of the log-likelihood, averaged over multiple identical experiments. In the present example, one can show that the Fisher information matrix is given by

$$\mathcal{I}_{ij}(\boldsymbol{\theta}) = \int dE \frac{\Phi_i(E)\Phi_j(E)}{\Phi_{\rm tot}(E|\boldsymbol{\theta})}. \tag{B3}$$

This matrix is equivalent to Eq. (2), where we used that further external constraints on the variance of the model parameters can be implemented by adding the inverse of the variance to the corresponding diagonal of the matrix.

The inverse of the Fisher matrix provides an approximation to the covariance matrix of the parameters of interest, which is used to derive the constraints and projections in this paper. The diagonal entries of $\mathcal{I}^{-1}$ hence provide estimates for the variance of the corresponding parameters, and their square root an estimate for the variance of the corresponding number of standard deviation. A one-sided 95% CL upper limit corresponds to 1.65 standard deviations, because integrating a standard normal Gaussian distribution from $-\infty$ to 1.65 yields 0.95, and hence, in our case $\sqrt{(\mathcal{I}^{-1})_{55}} = 1.65$. A 5σ detection, on the other hand, corresponds to 5 standard deviations and would therefore require a flux approximately three times larger than the upper limits presented in Figs. 3, 4 and 5. More details are presented in Ref. [27]. We tested our results with a conventional profile likelihood analysis [43], and find identical results.

---

[1] T. Bringmann and C. Weniger, Phys. Dark Univ. **1**, 194 (2012).
[2] M. Ackermann *et al.* (Fermi-LAT), Phys. Rev. D **91**, 122002 (2015).
[3] A. Abramowski *et al.* (H.E.S.S.), Phys. Rev. Lett. **110**, 041301 (2013).
[4] A. Boyarsky, O. Ruchayskiy, and M. Shaposhnikov, Annu. Rev. Nucl. Part. Sci. **59**, 191 (2009).
[5] K. N. Abazajian *et al.*, arXiv:1204.5379.
[6] E. Bulbul, M. Markevitch, A. Foster, R. K. Smith, M. Loewenstein, and S. W. Randall, Astrophys. J. **789**, 13 (2014).
[7] A. Boyarsky, O. Ruchayskiy, D. Iakubovskyi, and J. Franse, Phys. Rev. Lett. **113**, 251301 (2014).
[8] M. Srednicki, S. Theisen, and J. Silk, Phys. Rev. Lett. **56**, 263 (1986); **56**, 1883(E) (1986).
[9] S. Rudaz, Phys. Rev. Lett. **56**, 2128 (1986).
[10] L. Bergström, Nucl. Phys. **B325**, 647 (1989).
[11] A. Albert, G. A. Gomez-Vargas, M. Grefe, C. Munoz, C. Weniger, E. D. Bloom, E. Charles, M. N. Mazziotta, and A. Morselli (Fermi-LAT), J. Cosmol. Astropart. Phys. 10 (2014) 023.
[12] K. K. Boddy and J. Kumar, Phys. Rev. D **92**, 023533 (2015).
[13] K. K. Boddy and J. Kumar, in *9th International Conference on Interconnections between Particle Physics and Cosmology (PPC2015) Deadwood, SD, USA, June 29–July 03, 2015* (2016).
[14] K. K. Boddy, K. R. Dienes, D. Kim, J. Kumar, J.-C. Park, and B. Thomas, Phys. Rev. D **94**, 095027 (2016).
[15] J. Greiner *et al.*, Exp. Astron. **34**, 551 (2012).
[16] R. Essig, E. Kuflik, S. D. McDermott, T. Volansky, and K. M. Zurek, J. High Energy Phys. 11, 193 (2013).
[17] V. Tatischeff *et al.*, Proc. SPIE Int. Soc. Opt. Eng. **9905**, 99052N (2016).
[18] A. A. Moiseev *et al.*, arXiv:1508.07349.
[19] T. Sjöstrand, S. Mrenna, and P. Z. Skands, J. High Energy Phys. 05 (2006) 026.
[20] T. Sjöstrand, S. Ask, J. R. Christiansen, R. Corke, N. Desai, P. Ilten, S. Mrenna, S. Prestel, C. O. Rasmussen, and P. Z. Skands, Comput. Phys. Commun. **191**, 159 (2015).
[21] G. Corcella, I. G. Knowles, G. Marchesini, S. Moretti, K. Odagiri, P. Richardson, M. H. Seymour, and B. R. Webber, J. High Energy Phys. 01 (2001) 010.
[22] K. A. Olive *et al.* (Particle Data Group Collaboration), Chin. Phys. C **38**, 090001 (2014).
[23] V. N. Gribov and L. N. Lipatov, Yad. Fiz. **15**, 781 (1972) [Sov. J. Nucl. Phys. **15**, 438 (1972)].
[24] G. Altarelli and G. Parisi, Nucl. Phys. **B126**, 298 (1977).
[25] Y. L. Dokshitzer, Sov. Phys. Zh. Eksp. Teor. Fiz. **73**, 1216 (1977) [J. Exp. Theor. Phys. **46**, 641 (1977)].
[26] T. Sjöstrand, S. Mrenna, and P. Z. Skands, Comput. Phys. Commun. **178**, 852 (2008).
[27] T. Edwards and C. Weniger (to be published).
[28] J. Kndlseder, C.R. Phys. **17**, 663 (2016).
[29] A. W. Strong (Fermi-LAT), in Cosmic Rays for Particle and Astroparticle Physics, *Proceedings, 12th ICATPP Conference, Como, Italy, October 7–8, 2010* (2011), pp. 473–481.
[30] M. Ackermann *et al.* (Fermi-LAT), Phys. Rev. Lett. **115**, 231301 (2015).
[31] T. Bringmann, X. Huang, A. Ibarra, S. Vogl, and C. Weniger, J. Cosmol. Astropart. Phys. 07 (2012) 054.
[32] G. D. Kribs and E. T. Neil, Int. J. Mod. Phys. A **31**, 1643004 (2016).
[33] P. Cushman *et al.*, in *Proceedings, Community Summer Study 2013: Snowmass on the Mississippi (CSS2013): Minneapolis, MN, USA, July 29-August 6, 2013* (2013).
[34] R. Essig, J. Mardon, and T. Volansky, Phys. Rev. D **85**, 076007 (2012).
[35] R. Essig, A. Manalaysay, J. Mardon, P. Sorensen, and T. Volansky, Phys. Rev. Lett. **109**, 021301 (2012).
[36] R. Essig, M. Fernandez-Serra, J. Mardon, A. Soto, T. Volansky, and T.-T. Yu, J. High Energy Phys. 05 (2016) 046.
[37] Y. Hochberg, Y. Zhao, and K. M. Zurek, Phys. Rev. Lett. **116**, 011301 (2016).
[38] S. Profumo, Phys. Rev. D **93**, 055036 (2016).
[39] L. Wolz, M. Kilbinger, J. Weller, and T. Giannantonio, J. Cosmol. Astropart. Phys. 09 (**2012**) 009.
[40] S. Khedekar and S. Majumdar, J. Cosmol. Astropart. Phys. 02 (2013) 030.
[41] E. Sellentin, M. Quartin, and L. Amendola, Mon. Not. R. Astron. Soc. **441**, 1831 (2014).
[42] S. Camera, M. Fornasa, N. Fornengo, and M. Regis, J. Cosmol. Astropart. Phys. 06 (**2015**) 029.
[43] G. Cowan, K. Cranmer, E. Gross, and O. Vitells, Eur. Phys. J. C **71**, 1554 (2011); **73**, 2501(E) (2013).